HHS Public Access

Author manuscript

Am J Geriatr Psychiatry. Author manuscript; available in PMC 2018 June 08.

Published in final edited form as:

Am J Geriatr Psychiatry. 2018 June ; 26(6): 690–699. doi:10.1016/j.jagp.2018.03.003.

Association of hippocampal substructure resting-state functional connectivity with memory performance in older adults

Stephen F. Smagula, PhD[1,6], **Helmet T. Karim, PhD**[1], **Anusha Rangarajan, MS**[2], **Fernando Pasquini Santos, PhD**[3], **Sossena C. Wood, BS**[2], **Tales Santini, MS**[2], **John M. Jakicic, PhD**[4], **Charles F. Reynolds III, MD**[1], **Judy L. Cameron, PhD**[1], **Abbe N. Vallejo, PhD**[5], **Meryl A. Butters, PhD**[1], **Caterina Rosano, MD**[6], **Tamer S. Ibrahim, PhD**[2], **Kirk I Erickson, PhD**[7], and **Howard J. Aizenstein, MD PhD**[1]

[1]Department of Psychiatry, Western Psychiatric Institute and Clinic of University of Pittsburgh Medical Center, Pittsburgh, PA;

[2]Department of Bioengineering, University of Pittsburgh, Pittsburgh, PA;

[3]Faculty of Electrical Engineering, Federal University of Uberlândia, Uberlândia, MG, Brazil;

[4]Department of Health and Physical Activity, University of Pittsburgh, Pittsburgh, PA;

[5]Departments of Pediatrics and Immunology, University of Pittsburgh, Pittsburgh, PA;

[6]Department of Epidemiology, Graduate School of Public Health, University of Pittsburgh, Pittsburgh, PA;

[7]Departments of Psychology, University of Pittsburgh, Pittsburgh, PA;

Abstract

Objectives—Hippocampal hyperactivation marks pre-clinical dementia pathophysiology, potentially due to differences in the connectivity of specific medial temporal lobe structures. Our aims were to characterize the resting-state functional connectivity of medial temporal lobe sub-structures in older adults, and evaluate whether specific sub-structural (rather than global) functional connectivity relates to memory function.

Methods—In 15 adults (mean age=69 years), we evaluated the resting-state functional connectivity of medial temporal lobe sub-structures: dentate/Cornu Ammonis (CA)-4, CA-1, CA-2/3, subiculum, the molecular layer, entorhinal cortex, and parahippocampus. We used 7-Tesla Susceptibility Weighted Imaging and Magnetization-Prepared Rapid Gradient Echo sequences to segment substructures of the hippocampus, which were used as structural seeds for examining functional connectivity in a resting BOLD sequence. We then assessed correlations between functional connectivity with memory performance (short and long delay free recall on the California Verbal Learning Test or CVLT).

Corresponding author: Stephen F. Smagula Ph.D., Department of Psychiatry, University of Pittsburgh School of Medicine, 3811 O'Hara Street, Room E-1120, Pittsburgh, PA 15213, sfs26@pitt.edu, Phone: 412-246-5537.

Conflict of interests: The authors have no conflicts of interest to report.

Results—All the seed regions had significant connectivity within the temporal lobe (including the fusiform, temporal, and lingual gyri). The left CA1 was the only seeds with significant functional connectivity to the amygdala. The left entorhinal cortex was the only seed to have significant functional connectivity with frontal cortex (anterior cingulate and superior frontal gyrus). Only higher left dentate-left lingual connectivity was associated with poorer CVLT performance (Spearman r=−0.81, p=0.0003, Benjamini-Hochberg False Discovery Rate=0.01) after multiple comparison correction.

Conclusions—Rather than global hyper-connectivity of the medial temporal lobe, left dentate-lingual connectivity may provide a specific assay of medial temporal lobe hyper-connectivity relevant to memory in aging.

Biomarker models of dementia place elevated hippocampal (HC) activity in the earlier stages of pathogenesis and disease progression, followed by reductions in HC activity in later stages of illness (1–3). These models were derived from a range of neuroimaging evidence. Task-based neuroimaging studies have found HC hyperactivation related to memory: heightened hippocampal activation during memory tasks has been observed among individuals at risk for dementia (i.e., due to family history (4) or the apolipoprotein epsilon-4 gene (5, 6)); and in people with mild cognitive impairment, significant amyloid deposition is associated with greater hippocampal activation during memory tasks, which marks future risk of clinical progression (7). In addition, elevated resting-state HC connectivity within the default mode network is observed among older, compared with younger, adults (8); and among older adults, greater resting-state HC connectivity precedes future declines in memory performance.

However, there remains a need for a more anatomically fine-grained understanding of HC connectivity and how it is associated with variability in memory performance. Most prior research has focused on the longitudinal axis of the HC. This work has shown that the anterior hippocampus shares resting-state connectivity with entorhinal cortex and a lateral temporal network, whereas the posterior hippocampus shares connectivity with parahippocampus and posterior cingulate (9–11). But, as reviewed by Poppenk (12), differences between anterior and posterior functions may be due, in part, to differences in HC subfield composition along the longitudinal axis.

In the current work, we aimed to increase the anatomical specificity of past literature linking higher MTL activation with aging-related memory impairments (4–8). To do so, we first characterized the resting-state functional connectivity of medial temporal lobe (MTL) sub-structures in cognitively normal older adults. We expected to demonstrate that substructures had distinct connectivity patterns. We then evaluated whether worse memory performance was associated with the connectivity strength of specific or multiple substructures.

Methods

Study Design and Participants

Participants from Pittsburgh, Pennsylvania and surrounding areas were recruited starting March 2015. Eligible participants were between 60 and 85 years of age; participants who were at least 75 were also required to have no more than 12 years of education. The parent

study was focused on the effects of a physical intervention; however, the current report pertains only to the baseline assessments gathered before the intervention was conducted. To be included, participants had to be sedentary (defined as regular participation over the past 3 months in <60 minutes per week of moderate-to-vigorous leisure-time activity). Participants were also required to be able to walk a distance of at least 400 meters, and to have clearance from a physician for participating in the physical activity intervention and assessments. In addition, participants were required to be free from a history of stroke, uncontrolled hypertension, or other contraindications to moderate-intensity physical activity. Other exclusionary criteria were: evidence of dementia (based on participant report of a clinical diagnosis or modified mini mental status exam scores of less than 84); clinically significant depression symptoms (defined using the Patient Health Questionaire-9 cutpoint of ≥10); inability to undergo MRI; being unable to attend the intervention's sessions or plans to travel/relocate that would prevent attendance in at least 80% of the intervention sessions; current treatment for substance use disorder or consuming >1 alcoholic drink per day on >4 days per week; and being unwilling to provide blood samples (which were used in separate aims of this project). The University of Pittsburgh Institutional Review Board approved the study and all participants gave written and informed consent.

MRI Data Collection

Magnetic resonance images were acquired at the MR Research Center at the University of Pittsburgh on a 7-Tesla scanner (Magnetom, Siemens Medical Solutions, Erlangen Germany) using a customized 16/32-channel transmit/receive (respectively) head coil (13–16). A whole brain (excluding small portions of the frontal and occipital poles) Susceptibility Weighted Image (SWI: repetition time (TR)=1960ms, echo time (TE)=14ms, flip angle (FA)=60°, matrix size=1024×768, 64 slices, and 0.2×0.2×1.5mm resolution) was collected in the coronal plane along with an axial, whole brain 3D Magnetization-Prepared Rapid Gradient Echo (MPRAGE: TR=3000ms, TE=2.47ms, FA=6°, inversion time (TI)=1200ms, matrix size=280×320, 256 slices, and 0.7mm isotropic resolution) sequence. We also collected an axial, whole brain 7-minute resting-state functional echo planar (EPI) T2*-weighted sequence (fMRI; TR=2500ms, TE=20ms, FA=70°, matrix size=96×96, 52 slices, 155 volumes, and 2.3mm isotropic resolution with GeneRalized Autocalibrating Partial Parallel acquisition (GRAPPA) factor of 3). Participants were instructed to lie awake with their eyes open viewing a cross hair during the resting state sequence.

Structural Processing

We first bias-corrected SWI and MPRAGE images (separately) using statistical parametric mapping (SPM12) software. MTL substructures were then segmented using FreeSurfer Version 6.0 (http://surfer.nmr.mgh.harvard.edu/). We used FreeSurfer's longitudinal option to increase segmentation precision (17). Baseline and 6-month follow-up scans were used to create an unbiased within-subject template to initialize the segmentation of the baseline scans' HC, entorhinal cortex, and parahippocampus.

We then used FreeSurfer's HC subfield segmentation protocol (18) to perform a multi-spectral segmentation from the MPRAGE and SWI images (the latter of which provide increased contrast to identify subfields). We extracted the following seed regions from each

hemisphere: dentate gyrus (DG)/Cornu Ammonis (CA)-4, CA-2/3, CA-1, pre-subiculum/subiculum, and the molecular layer (of the CA and subiculum subfields, combined, per FreeSurfer's protocol). We combined DG/CA-4 because the CA-4 subfield lies within the dentate gyrus in FreeSurfer's HC subfield atlas (derived from high-resolution *ex-vivo* data) (18). CA-2 and CA-3 are combined in FreeSurfer's atlas due to a lack of distinguishing contrast between them. Pre-subiculum and subiculum were combined because they constitute the transition from three-layer HC cortex to six-layer cortex. Due to pronounced structural pathology (atrophy and cysts), one participant's subfield segmentations were inadequate, and they were excluded from further analysis (analytic sample n=15). An example segmentation is shown in Figure 1.

The MPRAGE was also included in the SPM12 pipeline for normalization of the functional imaging data. The MPRAGE was used to segment the brain into 6 tissue classes: gray and white matter, cerebrospinal fluid, and 3 non-brain tissue classes, which generated a deformation field that could be used to normalize or coregister to a standard anatomical space (Montreal Neurological Institute, MNI, space). An automatic mask for the intracranial volume was generated by thresholding the intracranial tissues with a probability of 0.1, filling the mask (imfill), and then performing a morphological closing operation (imclose, sphere of one voxel) in MatLab. These were visually inspected for accuracy. This mask (intracranial volume, ICV) was applied to the MPRAGE to remove non-brain tissues (which improves functional-structural coregistration).

Resting-State Processing

All processing was conducted using statistical parametric mapping (SPM12; http://www.fil.ion.ucl.ac.uk/spm/) in MatLab (MATLAB 2016b, The MathWorks, Natick, 2016). Interpolation was conducted using 4th degree B-spline interpolation unless otherwise noted. Resting-state fMRI images were slice time corrected (middle slice was used as reference) and motion corrected (rigid-body coregistration to the mean with mutual information similarity metric). Spike artifacts were removed using a previously established method that uses wavelets to filter spike artifacts (19). We have not performed motion scrubbing as the wavelet despiking method automatically removes filters spike artifacts associated with motion. Five principal components of white matter and cerebrospinal fluid were extracted using principal components analysis (PCA), which finds an orthogonal (i.e., uncorrelated) set of time series that explain a certain proportion of the variance of the original set of time series (i.e., the entire set of time series in the white matter and CSF). Using Monte-Carlo simulations, past studies have shown that approximately 5-6 components is sufficient to explain a significant proportion of the variance across the white matter and CSF (20). These 5 principal components as well as 6 motion parameters and a vector to model the global mean of the time series. Band-pass filtering was conducted by including several regressors that represented cosines with all discrete frequencies except those within the standard expected resting state frequencies (0.008 to 0.15 Hz). This was done such that the procedure is done in one step as part of the regression (SPM conducts its high-pass filtering similarly). This processing removed variance associated with motion, global signals from white matter and CSF as well as the global mean, and frequencies of no interest, respectively.

To coregister the middle temporal gyrus sub-structures into native fMRI space, the skull-stripped MPRAGE was then coregistered to the mean functional image (affine transformation) that was applied to the structural segmentations (nearest neighbor interpolation). The principle time series was extracted (using principal components analysis) for each of the regions described and a connectivity map (correlation between the region's time series and each voxel-wise time series) was generated for each region. These connectivity maps were generated in native fMRI space. They were next transformed to standard MNI space.

To normalize the connectivity maps into MNI space, the mean functional image was used to compute the (affine) transformation between the functional images and the skull-stripped MPRAGE, which was applied to each connectivity map. The deformation field was then applied to each connectivity map to normalize them into MNI space. Finally, each map was smoothed using a Gaussian kernel with full-width at half-maximum (FWHM) of 8mm.

Participants during the study had some motion. We evaluated the max translational motion [3.0 (2.4)], max range of translational motion [3.7 (2.6)], average root mean square (RMS) motion [1.6 (1.2)], average scan-to-scan motion [0.4 (0.2)], and percent of volumes classified as 'head jerks' [23.0 (19.3) or approximately 35 volumes on average]. Head jerks were identified and interpolated using the wavelet despiking method described above. To prevent from analyzing connectivity measures that are potentially due to motion, we discarded aspects connectivity that had any statistically significant (uncorrected $p<0.05$) Spearman correlations with the above-listed motion parameters.

Memory assessments

The second-edition California Verbal Learning Test (21) was used to derive two memory measures: short-delay free recall and long-delay free recall. In the short-delay condition, participants were read a list of 16 nouns and were then asked to recall as many of the words as possible. In the long-delay condition, participants were again asked to recall as many words as possible after a 20-minute delay. We chose the short- and long-delay free recall of the CVLT-2 list as the best measures representing the ability to acquire new explicit memories and importantly, retain the information over time, a function mediated by the hippocampus.

Statistical Analyses

We performed a voxel-wise statistical group analysis for each connectivity map using statistical non-parametric mapping (SnPM13) (22), which computes non-parametric p-values (23) which are then corrected using a cluster-wise inference method (cluster forming threshold of $p<0.001$) that controls the family wise error rate (FWE) at $\alpha=0.05$ (24). We have done this due to recent work that states that parametric p-values combined with cluster based multiple comparisons corrections do not sufficiently control for type I error (25). We performed a one-sample t-test across all participants for each region correlation map (parameter estimate of the correlation) to find brain regions that were correlated with the seed region time series (test for regions whose parameter estimate is significantly greater than zero). For each region with significant connectivity outside of the seeds, we extracted

the strength of connectivity. Finally, we tested whether each aspect of connectivity was associated with memory performance using Spearman correlations. Since there were 20 regions where the seeds had significant connectivity, we corrected for assessing multiple connectivity-memory correlations by defining statistical significance as a Benjamini-Hochberg False Discover Rate $q<0.05$ (treating short-delay and long-delay memory measures as separate comparison sets).

Results

Sample characteristics

The 15 participants (14 females and 1 male, average of 69.5 years old, standard deviation (SD)=3.6) had an average of 15.8 years of education (SD=2.7). Almost all (93% or 14/15) of participants were white. Average scores on the long and short free recall tasks, respectively, were 10.3 (SD=3.4) and 10.3 (SD=3.4).

Resting-state connectivity

All sub-structural seeds had significant functional connectivity with temporal regions such as the fusiform, temporal, and lingual gyri. The connectivity strength of each ROI to other regions are shown in Supplemental Table 1. The connectivity between the seeds and other regions was distinct (Figures 2 and 3): the left CA1 was the only subfield that had significant connectivity with the left amygdala; the left entorhinal cortex was the only seed region that had significant connectivity with the frontal cortex (medial areas of the right anterior cingulate and superior frontal gyri); and the left DG and left subiculum were the only regions that had significant connectivity with calcarine cortex. Some seeds also had connectivity with cerebellar regions.

Associations of connectivity with memory performance

Greater connectivity between the left DG seed and the left lingual gyrus was associated with poorer long-delay memory performance ($n=15$, Spearman $r=-0.81$, $p=0.0003$, $q=0.01$; Figure 4). Age, education, and motion parameters did not correlate with the strength of connectivity between the left DG and left lingual gyrus, and adjustment for these factors did not attenuate the correlation between connectivity and long delay free recall memory performance. No other seed regions had connectivity that was associated with memory performance after multiple-comparison correction (Supplemental Tables 2 and 3). None of the connectivity aspects that were excluded (due to correlating with motion) were significantly associated with memory performance.

Discussion

In cognitively healthy older adults, we found MTL structures had resting-state functional connectivity with other temporal regions and hubs of the DMN. By characterizing patterns of connectivity across subregions, we identified that only the left entorhinal cortex had significant resting-state functional connectivity with anterior (frontal) DMN. Left subiculum and dentate had connectivity with posterior DMN (around the calcarine sulcus). These findings add strength to Poppenk's (12) argument that differences in subfield composition

across the longitudinal axis could bias functional connectivity of the anterior and posterior segments.

These findings are consistent with, and add anatomical specificity to, prior neuroimaging research from younger adult samples (9–11, 26, 27). We found the dentate and subiculum had connectivity with a posterior node around the calcarine sulcus: posterior hippocampus, which is thought to be composed more of dentate than CA fields, has functional connectivity with posterior nodes of the DMN network (12); and previous work also found functional connectivity of the subiculum with posterior default mode network hubs (28). Our findings are plausible given electrophysiological and anatomical tracer studies (reviewed in (29)); these past studies demonstrate association areas connect to entorhinal cortex, which inputs on the HC tri-synaptic circuit, in turn outputting primarily through the subiculum.

We also found greater left DG-lingual cortex connectivity was associated with worse short- and long-term explicit memory performance. This may result from a loss of inhibitory protein expression in interneurons (30–32). Our findings add anatomical specificity to past literature, which indicates higher MTL activation, is associated with aging-related memory impairments (4–8). Previous high-resolution neuroimaging research found higher DG/CA3 activation during tasks requiring pattern separation in nondemented older adults (33) and adults with Mild Cognitive Impairment (34). Pattern separation, occurring primarily in the DG, enables distinct events to be coded and remembered separately (35). The lingual gyrus is a critical node in semantic information processing (36), and a semantic processing network is active during rest (37). Higher resting left DG-left lingual connectivity may thus reflect inefficient parsing of semantic information, which could limit the capacity to meet episodic memory task demands, or create interference during explicit memory encoding.

Several limitations of our study should be noted. These findings may not necessarily generalize to other populations because we focused here on a small sample of physically and cognitively healthy older adults and almost all white females. Due to the small sample size, it is possible that there exist other regions that moderately correlate with these substructures, but were not detected due to lack of statistical power. While the structural imaging was sub-millimeter, the resting state was a lower resolution – thus it is possible that some of the specificity of the subfield connectivity is lost. This resolution is lowered even more due to the large smoothing kernel (8mm FWHM), which was chosen due to the aging cohort and differences in brain structure. Our analyses were designed to identify the whole-brain connectivity of the predominate functional signal found within anatomically defined substructures, but future work is needed to further delineate functionally distinct signals within these sub-structures (as in data-driven work e.g., (10, 28)). We also have not assessed how these networks respond to cognitive tasks. Furthermore, we examined the functional connectivity between MTL substructures and the rest of the brain, and cannot make inferences regarding the temporal dynamics of these functional systems.

In conclusion, we have documented differences in the connectivity of MTL substructures at rest in healthy older adults. Rather than global hippocampal hyperconnectivity being related to worse memory in aging, left dentate-lingual connectivity strength may provide a specific assay relevant to memory. Strengths of our study include the use of 7-Telsa neuroimaging

sequences that provide adequate resolution and contrast, along with refined multispectral segmentation methods (18), which allowed us to distinguish the DG and other sub-regions. Future work is needed to replicate these findings, clarify the temporal dynamics of these networks (e.g., using dynamic causal modeling), and understand their pathogenic basis. Specifically, longitudinal studies in larger, diverse sample of older adults are needed to understand how these networks relate to other aging-related disease processes, and specifically to modifiable risk factors.

Supplementary Material

Refer to Web version on PubMed Central for supplementary material.

Acknowledgments

The Healthy Brain Aging Study was supported by the Aging Institute of UPMC Senior Services and the University of Pittsburgh. In completing this work, SFS has been supported by T32 HL082610, T32 MH019986, and K01 MH112683. Additional support was provided by R01 AG053952, R01 CA196762, R01 DK095172, and P30 AG024827 to KIE.

References

1. Leal SL, Yassa MA. Perturbations of neural circuitry in aging, mild cognitive impairment, and Alzheimer's disease. Ageing research reviews. 2013; 12:823–831. [PubMed: 23380151]
2. Aizenstein HJ, Klunk WE. Where is hippocampal activity in the cascade of Alzheimer's disease biomarkers? Brain: a journal of neurology. 2015; 138:831–833. [PubMed: 25802317]
3. Sperling RA, Aisen PS, Beckett LA, et al. Toward defining the preclinical stages of Alzheimer's disease: Recommendations from the National Institute on Aging-Alzheimer's Association workgroups on diagnostic guidelines for Alzheimer's disease. Alzheimer's & dementia: the journal of the Alzheimer's Association. 2011; 7:280–292.
4. Bassett SS, Yousem DM, Cristinzio C, et al. Familial risk for Alzheimer's disease alters fMRI activation patterns. Brain: a journal of neurology. 2006; 129:1229–1239. [PubMed: 16627465]
5. Bookheimer SY, Strojwas MH, Cohen MS, et al. Patterns of brain activation in people at risk for Alzheimer's disease. The New England journal of medicine. 2000; 343:450–456. [PubMed: 10944562]
6. Filippini N, MacIntosh BJ, Hough MG, et al. Distinct patterns of brain activity in young carriers of the APOE-epsilon4 allele. Proc Natl Acad Sci U S A. 2009; 106:7209–7214. [PubMed: 19357304]
7. Huijbers W, Mormino EC, Schultz AP, et al. Amyloid-β deposition in mild cognitive impairment is associated with increased hippocampal activity, atrophy and clinical progression. Brain: a journal of neurology. 2015; 138:1023–1035. [PubMed: 25678559]
8. Salami A, Pudas S, Nyberg L. Elevated hippocampal resting-state connectivity underlies deficient neurocognitive function in aging. Proc Natl Acad Sci U S A. 2014; 111:17654–17659. [PubMed: 25422457]
9. Kahn I, Andrews-Hanna JR, Vincent JL, et al. Distinct Cortical Anatomy Linked to Subregions of the Medial Temporal Lobe Revealed by Intrinsic Functional Connectivity. Journal of Neurophysiology. 2008; 100:129–139. [PubMed: 18385483]
10. Libby LA, Ekstrom AD, Ragland JD, et al. Differential connectivity of perirhinal and parahippocampal cortices within human hippocampal subregions revealed by high-resolution functional imaging. The Journal of neuroscience: the official journal of the Society for Neuroscience. 2012; 32:6550–6560. [PubMed: 22573677]
11. Poppenk J, Moscovitch M. A hippocampal marker of recollection memory ability among healthy young adults: contributions of posterior and anterior segments. Neuron. 2011; 72:931–937. [PubMed: 22196329]

12. Poppenk J, Evensmoen HR, Moscovitch M, et al. Long-axis specialization of the human hippocampus. Trends in Cognitive Sciences. 2013; 17:230–240. [PubMed: 23597720]
13. Kim J, Santini T, Bae KT, et al. Development of a 7 T RF coil system for breast imaging. NMR in biomedicine. 2017; 30
14. Kim J, Krishnamurthy N, Santini T, et al. Experimental and numerical analysis of B1+ field and SAR with a new transmit array design for 7T breast MRI. Journal of Magnetic Resonance. 2016; 269:55–64. [PubMed: 27240143]
15. Ibrahim, TST., Raval, S., Krishnamurthy, N., Wood, S., Kim, J., Zhao, Y., Wu, X., Yacoub, E., Aizenstein, H., Zhao, T. Towards Homogenous 7T Neuro Imaging: Findings and Comparisons between 7T TTT and NOVA RF Coil Systems. Honolulu, Hawaii, USA: 2017.
16. Ibrahim, TS., Zhao, T., Krishnamurthy, N., Raval, SB., Zhao, T., Wood, S., Kim, J. 20-To-8 Channel Tx Array with 32-Channel Adjustable Receive-Only Insert for 7T Head Imaging. Salt Lake City, Utah, USA: 2013.
17. Reuter M, Schmansky NJ, Rosas HD, et al. Within-subject template estimation for unbiased longitudinal image analysis. NeuroImage. 2012; 61:1402–1418. [PubMed: 22430496]
18. Iglesias JE, Augustinack JC, Nguyen K, et al. A computational atlas of the hippocampal formation using ex vivo, ultra-high resolution MRI: Application to adaptive segmentation of in vivo MRI. NeuroImage. 2015; 115:117–137. [PubMed: 25936807]
19. Patel AX, Kundu P, Rubinov M, et al. A wavelet method for modeling and despiking motion artifacts from resting-state fMRI time series. NeuroImage. 2014; 95:287–304. [PubMed: 24657353]
20. Behzadi Y, Restom K, Liau J, et al. A Component Based Noise Correction Method (CompCor) for BOLD and Perfusion Based fMRI. NeuroImage. 2007; 37:90–101. [PubMed: 17560126]
21. Delis, DCKJ., Kaplan, E., Ober, BA. California Verbal Learning Test®. Second. San Antonio, TX: Psychological Corporation; 2000. CVLT® -II
22. Nichols TE, Holmes AP. Nonparametric permutation tests for functional neuroimaging: a primer with examples. Human brain mapping. 2002; 15:1–25. [PubMed: 11747097]
23. Holmes AP, Blair RC, Watson JD, et al. Nonparametric analysis of statistic images from functional mapping experiments. J Cereb Blood Flow Metab. 1996; 16:7–22. [PubMed: 8530558]
24. Nichols TE, Holmes AP. Nonparametric permutation tests for functional neuroimaging: a primer with examples. Human brain mapping. 2002; 15:1–25. [PubMed: 11747097]
25. Eklund A, Nichols TE, Knutsson H. Cluster failure: Why fMRI inferences for spatial extent have inflated false-positive rates. Proc Natl Acad Sci U S A. 2016; 113:7900–7905. [PubMed: 27357684]
26. Greicius MD, Srivastava G, Reiss AL, et al. Default-mode network activity distinguishes Alzheimer's disease from healthy aging: Evidence from functional MRI. Proceedings of the National Academy of Sciences of the United States of America. 2004; 101:4637–4642. [PubMed: 15070770]
27. Wagner G, Gussew A, Köhler S, et al. Resting state functional connectivity of the hippocampus along the anterior–posterior axis and its association with glutamatergic metabolism. Cortex. 2016; 81:104–117. [PubMed: 27182810]
28. Chase HW, Clos M, Dibble S, et al. Evidence for an anterior-posterior differentiation in the human hippocampal formation revealed by meta-analytic parcellation of fMRI coordinate maps: focus on the subiculum. NeuroImage. 2015; 113:44–60. [PubMed: 25776219]
29. Lavenex P, Amaral DG. Hippocampal-neocortical interaction: a hierarchy of associativity. Hippocampus. 2000; 10:420–430. [PubMed: 10985281]
30. Geinisman Y, deToledo-Morrell L, Morrell F, et al. Age-related loss of axospinous synapses formed by two afferent systems in the rat dentate gyrus as revealed by the unbiased stereological dissector technique. Hippocampus. 1992; 2:437–444. [PubMed: 1308200]
31. Spiegel AM, Koh MT, Vogt NM, et al. Hilar Interneuron Vulnerability Distinguishes Aged Rats With Memory Impairment. The Journal of comparative neurology. 2013; 521:3508–3523. [PubMed: 23749483]

32. Koh MT, Haberman RP, Foti S, et al. Treatment Strategies Targeting Excess Hippocampal Activity Benefit Aged Rats with Cognitive Impairment. Neuropsychopharmacology. 2010; 35:1016–1025. [PubMed: 20032967]

33. Yassa MA, Lacy JW, Stark SM, et al. Pattern separation deficits associated with increased hippocampal CA3 and dentate gyrus activity in nondemented older adults. Hippocampus. 2011; 21:968–979. [PubMed: 20865732]

34. Yassa MA, Stark SM, Bakker A, et al. High-resolution structural and functional MRI of hippocampal CA3 and dentate gyrus in patients with amnestic Mild Cognitive Impairment. NeuroImage. 2010; 51:1242–1252. [PubMed: 20338246]

35. Berron D, Schutze H, Maass A, et al. Strong Evidence for Pattern Separation in Human Dentate Gyrus. The Journal of neuroscience: the official journal of the Society for Neuroscience. 2016; 36:7569–7579. [PubMed: 27445136]

36. Ghosh S, Basu A, Kumaran SS, et al. Functional mapping of language networks in the normal brain using a word-association task. The Indian Journal of Radiology & Imaging. 2010; 20:182–187. [PubMed: 21042440]

37. Jackson RL, Hoffman P, Pobric G, et al. The Semantic Network at Work and Rest: Differential Connectivity of Anterior Temporal Lobe Subregions. The Journal of Neuroscience. 2016; 36:1490–1501. [PubMed: 26843633]

Highlights

- Greater medial temporal lobe functional engagement is associated with pre-clinical dementia pathophysiology.
- We do not know whether these processes are related to global or anatomically specific aspects of medial temporal lobe function.
- We characterized the resting-state functional connectivity of medial temporal lobe substructures to identify which aspect(s) correlate with memory performance.
- Left dentate-lingual gyri connectivity strongly correlated with memory performance, whereas the other aspects of medial temporal lobe connectivity did not.
- Rather than global hyperconnectivity, higher left dentate-lingual gyri connectivity specifically marks pre-clinical variability in memory performance.

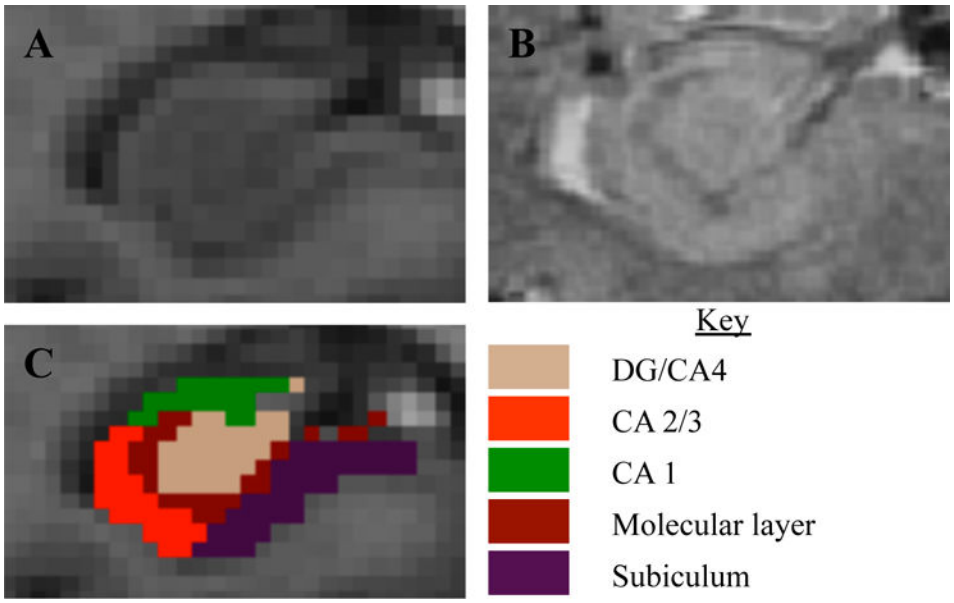

Figure 1.

Hippocampal images and segmentation from one participant. (A) MPRAGE image, and (B) SWI image zoomed onto the right hippocampus, with (C) showing the segmentation produced from the FreeSurfer 6.0 multispectral pipeline. Note the resolution and contrast is much higher for the SWI, compared with the MPRAGE, which allowed for identification of the granular cell layer and segmentations based on image features rather than geometric rules.

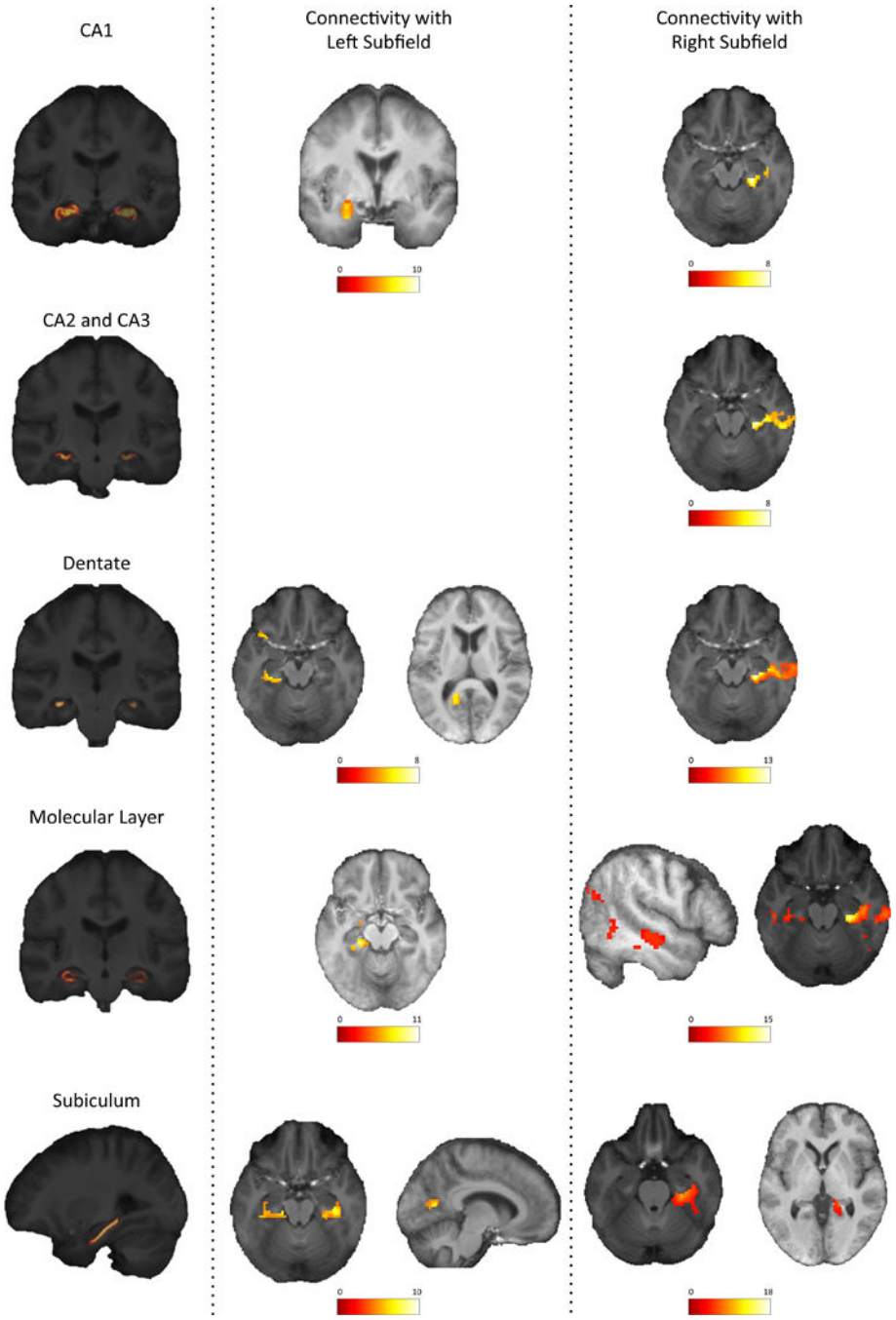

Figure 2.
Resting-state functional connectivity of hippocampal substructures.

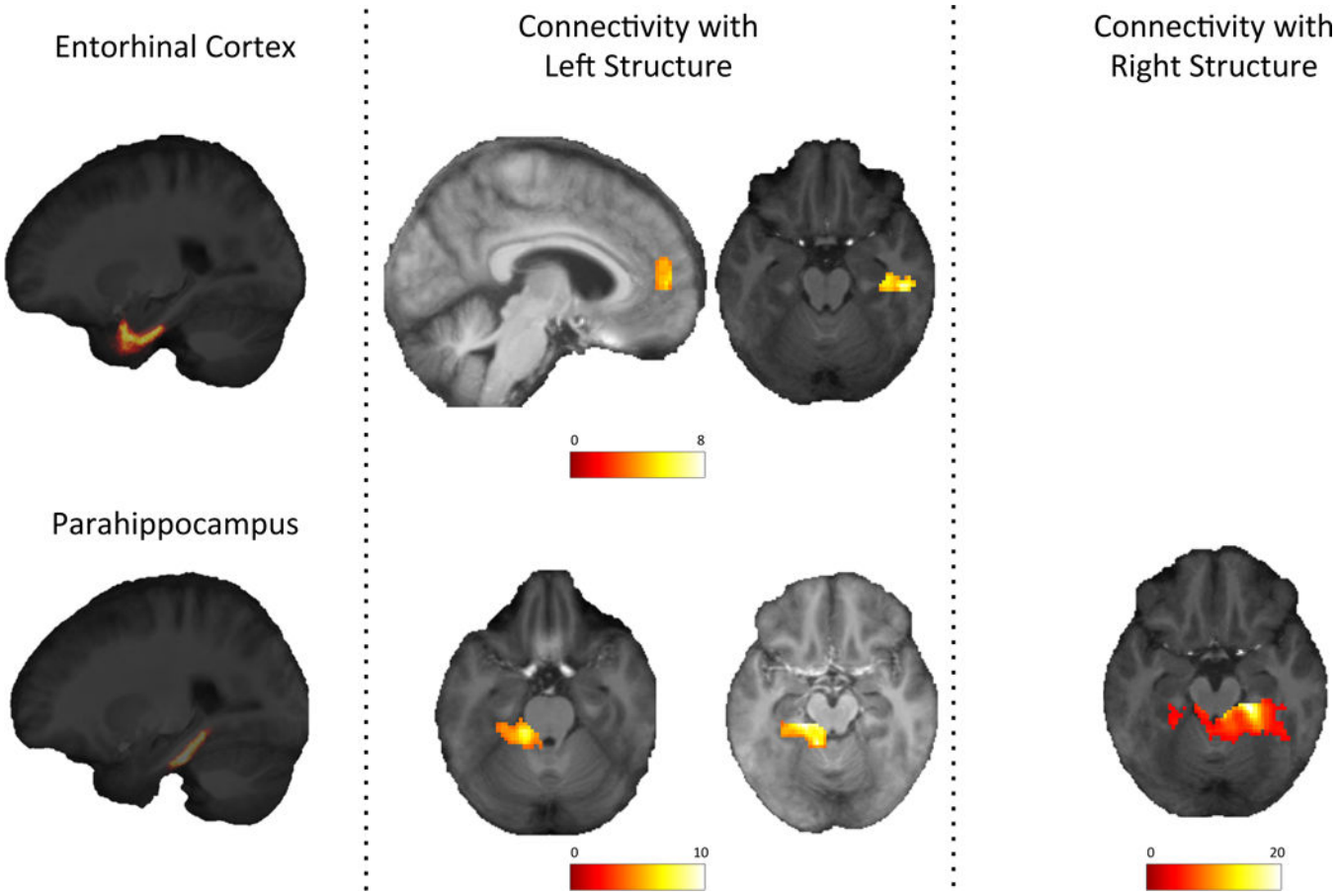

Figure 3.
Resting-state functional connectivity of entorhinal and parahippocampal cortex

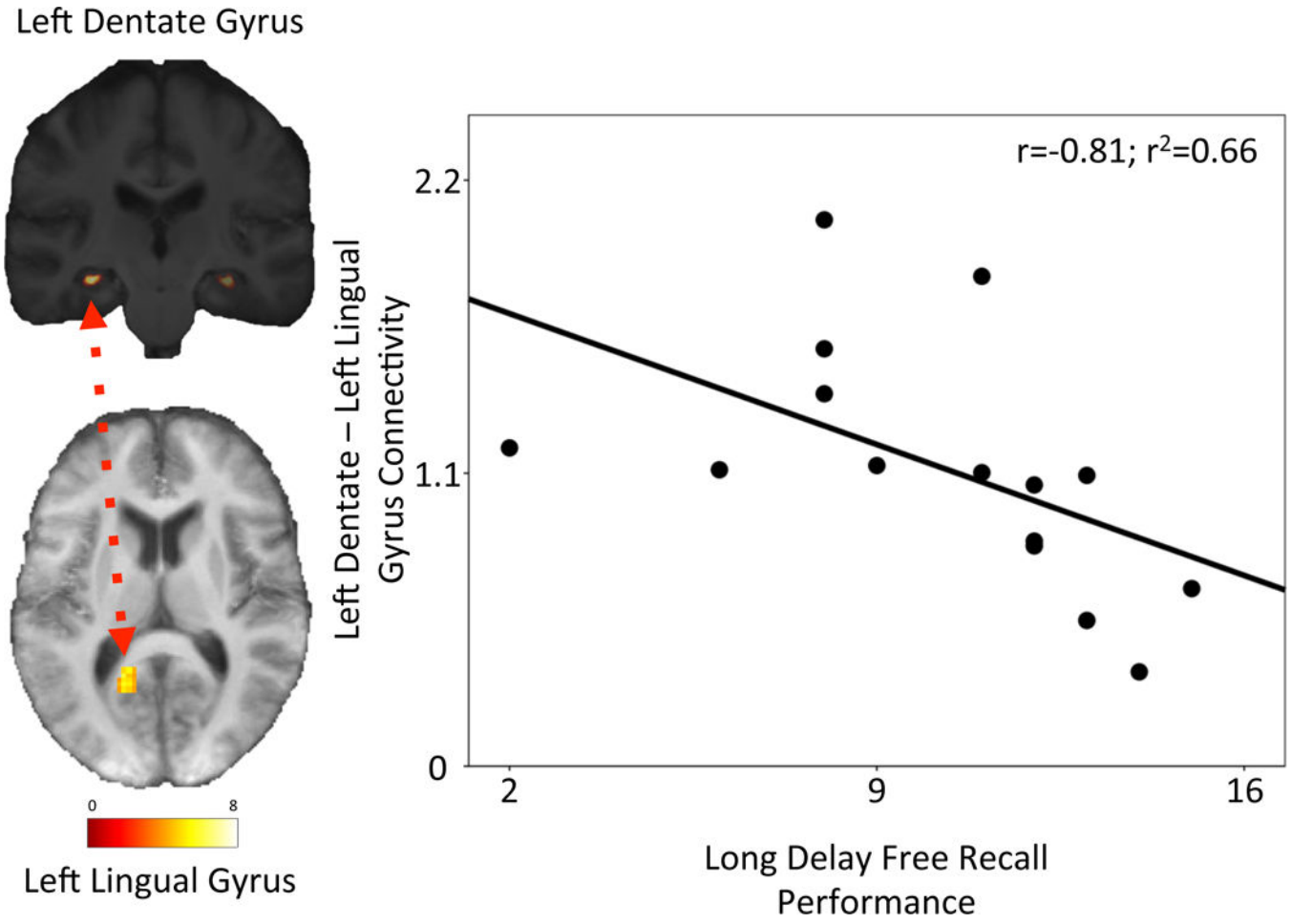

Figure 4.
Left dentate-left lingual gyrus functional connectivity correlates with memory performance.